Tl–Ca–Ba–Cu–O superconducting oxides

by R. B. Beyers
S. S. P. Parkin
V. Y. Lee
A. I. Nazzal
R. J. Savoy
G. L. Gorman
T. C. Huang
S. J. La Placa

This paper reviews structural studies of Tl–Ca–Ba–Cu–O superconducting oxides by the authors and others and points out directions for future work.

Introduction

The discovery by Bednorz and Müller [1, 2] of superconductivity above 30 K in $La_{2-x}Ba_xCuO_4$ sparked an intense search for other superconducting oxides. Researchers found new families of layered copper oxides displaying high-temperature superconductivity in the Ln–Ba–Cu–O [3], Bi–Ca–Sr–Cu–O [4], Tl–Ca–Ba–Cu–O [5, 6], and Pb–Ln–Sr–Cu–O [7] systems (where Ln = lanthanide). Of these, the Tl–Ca–Ba–Cu–O system has the widest range of crystal structures and properties: seven different oxides have been prepared thus far, with properties ranging from nonsuperconducting to superconducting at 125 K (see Figure 1 and Table 1, shown later). This paper reviews the many structural studies [8–54] of Tl–Ca–Ba–Cu–O oxides. We begin by discussing the methods used to prepare these materials. For convenience, we divide the structural studies into four separate categories: basic crystal structures, superstructures, defect structures, and site occupancy. In each section we try to distinguish clearly between facts that are generally known and areas where more research is needed.

Materials preparation

The thermodynamics and kinetics of phase formation in the thallium system remain largely unknown. Nonetheless, several "recipes" have been found for making ceramic samples. In our studies [9–12], samples were prepared by thoroughly mixing Tl_2O_3, CaO, BaO_2, and CuO powders. After grinding, the mixtures were pressed into pellets and wrapped in gold. The pellets were fired at 880 C for 3 h in sealed quartz tubes initially containing one atmosphere oxygen, then furnace-cooled to room temperature over a 4 h period. Although the resulting samples were multiphase, one phase would be predominant (>60%), and each of the secondary phases (mainly Ba and Ca copper oxides) comprised no more than 15% of the sample. Combined electron microprobe, X-ray diffraction, and transmission electron microscopy studies of these materials enabled us to deduce the basic crystallography and microstructure of six different oxides.

Not surprisingly, the phases formed depend on the starting composition, the use of a closed or open reactor, the annealing treatment, and the thallium and oxygen partial pressures. However, at the present time, there is no detailed understanding of the interplay among these processing variables. For example, initial studies by both Hazen et al. [8] and Parkin et al. [9] reported that a starting composition of 2 Tl: 2 Ca: 2 Ba: 3 Cu yields predominantly the $Tl_2Ca_1Ba_2Cu_2O_8$ phase, rather than the expected $Tl_2Ca_2Ba_2Cu_3O_{10}$ phase. More recently, we found that the composition of the major phase more closely matches the starting composition when slower cooling rates are used [12]. A second puzzling example concerns the formation of $Tl_1Ca_3Ba_2Cu_4O_{11}$. For samples prepared in flowing oxygen, Sugise et al. [42] reported that $Tl_2Ca_2Ba_2Cu_3O_{10}$ forms first, followed by $Tl_1Ca_2Ba_2Cu_3O_9$, which with further sintering transforms to $Tl_1Ca_3Ba_2Cu_4O_{11}$. The conversion from

Table 1 Measured properties of Tl–Ca–Ba–Cu oxides [11, 12, 40].

Name	*Composition*	*Symmetry*	*Lattice parameters* (Å)	*Superlattice wave vector*	T_c (K)
1021	$Tl_{1.2}Ba_2Cu_{0.7}O_{4.8}$	*P4/mmm*	$a = 3.869$ (2) $c = 9.694$ (9)	*	†
1122	$Tl_{1.1}Ca_{0.9}Ba_2Cu_{2.1}O_{7.1}$	*P4/mmm*	$a = 3.8505$ (7) $c = 12.728$ (2)	$\langle 0.29, 0, 0.5 \rangle$	65–85
1223	$Tl_{1.1}Ca_{1.8}Ba_2Cu_{3.0}O_{9.7}$	*P4/mmm*	$a = 3.8429$ (6) $c = 15.871$ (3)	$\langle 0.29, 0, 0.5 \rangle$	100–110
1324	$Tl_1Ca_3Ba_2Cu_4O_{11}$	*P4/mmm*	$a = 3.85$ $c = 19.1$	*	122
2021	$Tl_{1.9}Ba_2Cu_{1.1}O_{6.4}$	*Fmmm*‡	$a = 5.445$ (2) $b = 5.492$ (1) $c = 23.172$ (6)	$\langle \overline{0.08}, 0.24, 1 \rangle$	†
	$Tl_{1.8}Ca_{0.02}Ba_2Cu_{1.1}O_{6.3}$	*I4/mmm*‡	$a = 3.8587$ (4) $c = 23.152$ (2)	$\langle \overline{0.16}, 0.08, 1 \rangle$	20–80
2122	$Tl_{1.7}Ca_{0.9}Ba_2Cu_{2.3}O_{8.1}$	*I4/mmm*	$a = 3.857$ (1) $c = 29.39$ (1)	$\langle 0.17, 0, 1 \rangle$	95–108
2223	$Tl_{1.6}Ca_{1.8}Ba_2Cu_{3.1}O_{10.1}$	*I4/mmm*	$a = 3.822$ (4) $c = 36.26$ (3)	$\langle 0.17, 0, 1 \rangle$	118–125

*No superlattice modulations have been observed in these crystals thus far.
† Nonmetallic or weakly metallic samples with no superconducting transition observed down to 4.2 K.
‡ Taking the superlattice into account lowers the symmetry of this structure to monoclinic, with the *c* axis being the unique axis.

$Tl_2Ca_2Ba_2Cu_3O_{10}$ to $Tl_1Ca_2Ba_2Cu_3O_{10}$ can be easily explained by thallium loss to the gas stream. The second transformation is more difficult to explain. Sugise et al. [42] suggest that the excess cations may be absorbed in an amorphous phase.

Similar processing problems arise in the synthesis of thin films [13, 30, 54]. The cation stoichiometries can be readily controlled during deposition. Control of the thallium and oxygen partial pressures during the subsequent heat treatment then determines which oxides form. Interdiffusion and reaction with the substrate are additional concerns during thin-film preparation.

Determining the high-temperature chemistry of a quinary system is a difficult task. The volatility and toxicity of thallium make the job that much harder, yet a better understanding of this area is critical for producing higher-quality materials for applications and for experimentation.

Basic crystal structures

Hazen et al. [8] identified three oxides in the samples of Sheng and Hermann [5, 6]: $Tl_2Ba_2Cu_1O_6$, $Tl_2Ca_1Ba_2Cu_2O_8$, and $Tl_2Ca_2Ba_2Cu_3O_{10}$. For brevity, these phases are referred to as 2021, 2122, and 2223, respectively. As shown in **Figure 1**, these oxides are made up of Cu perovskite-like units containing one, two, and three CuO_2 planes separated by Tl–O bilayers. 2122 and 2223 have body-centered tetragonal structures. The convergent-beam electron diffraction patterns in **Figures 2(a)** and **2(b)** show that these crystals are indeed tetragonal. On the other hand, 2021 has two polymorphs, one nominally face-centered orthorhombic and the other nominally body-centered tetragonal [11, 12, 38, 39]. The orthorhombic 2021 crystals are highly twinned. For these crystals, the unit cell axes in Figure 1(e) should be rotated ~45° about the *c* axis and the unit cell redefined with $a \sim b \sim 2a_p$, where $a_p \sim 3.85$ Å (see **Table 1**).

Parkin et al. [10] subsequently discovered three additional oxides in which the Cu perovskite-like units are separated by Tl–O *monolayers*, rather than by Tl–O *bilayers*: $Tl_1Ba_2Cu_1O_5$, $Tl_1Ca_1Ba_2Cu_2O_7$, and $Tl_1Ca_2Ba_2Cu_3O_9$. More recently, Ihara et al. [40] prepared the fourth member of this series, $Tl_1Ca_3Ba_2Cu_4O_{11}$. For brevity, these phases are referred to as 1021, 1122, 1223, and 1324, respectively. All of these Tl–O monolayer structures have primitive tetragonal cells.

The Bi–Ca–Sr–Cu–O system contains analogs of the Tl–O bilayer structures, but not the Tl–O monolayer structures. Thus the Tl–Ca–Ba–Cu–O system has the unique ability to vary both the size and the separation of the Cu perovskite-like units, which may allow the role of coupling between successive Cu perovskite-like units to be examined. The nominal compositions and structures for all seven oxides are summarized in Table 1.

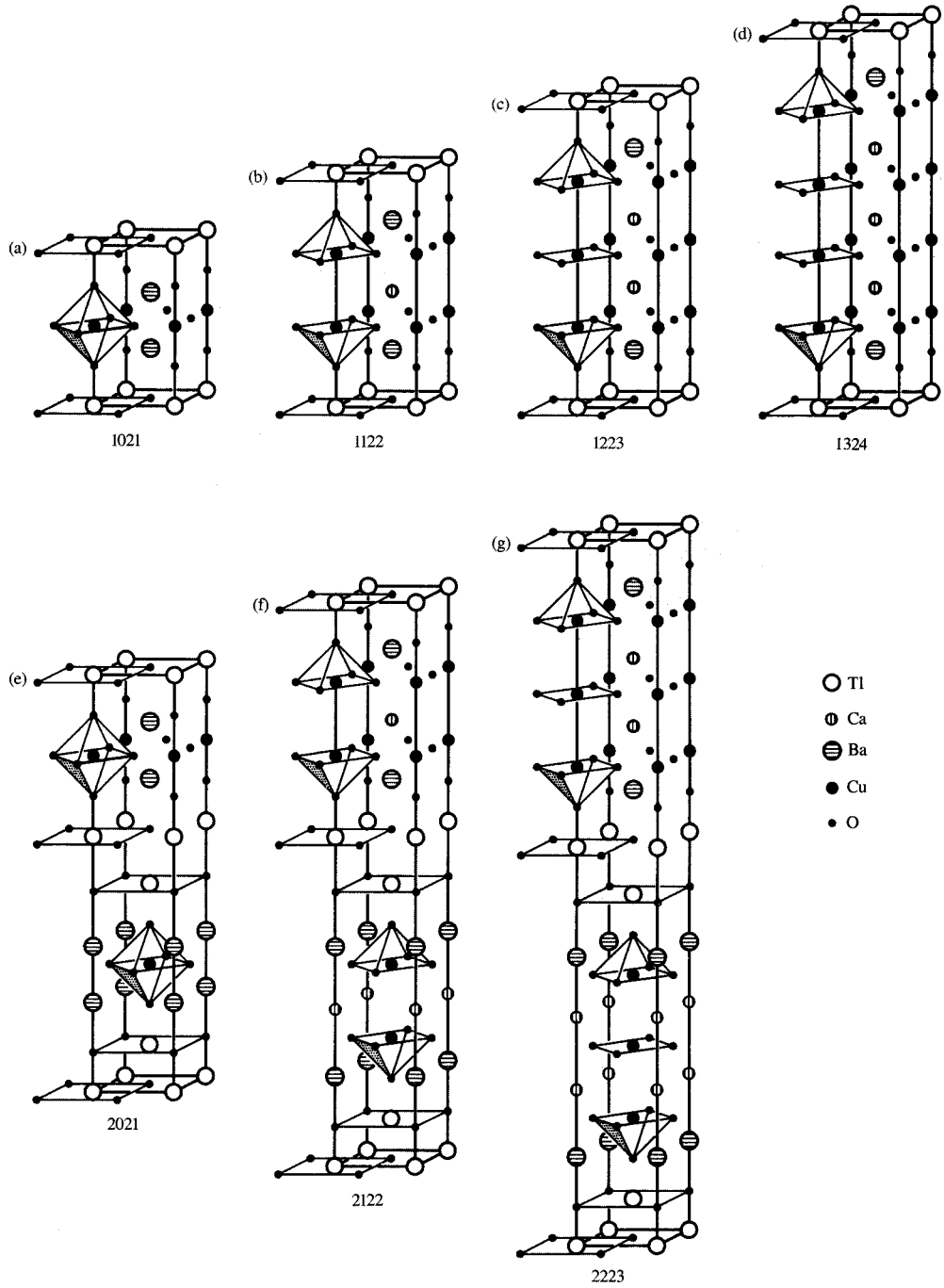

Figure 1

Nominal unit cells for (a) $Tl_1Ba_2Cu_1O_5$, (b) $Tl_1Ca_1Ba_2Cu_2O_7$, (c) $Tl_1Ca_2Ba_2Cu_3O_9$, (d) $Tl_1Ca_3Ba_2Cu_4O_{11}$, (e) $Tl_2Ba_2Cu_1O_6$, (f) $Tl_2Ca_1Ba_2Cu_2O_8$, and (g) $Tl_2Ca_2Ba_2Cu_3O_{10}$. Note that the Ca and Ba positions in the chemical formula are often reversed in the literature [11, 40].

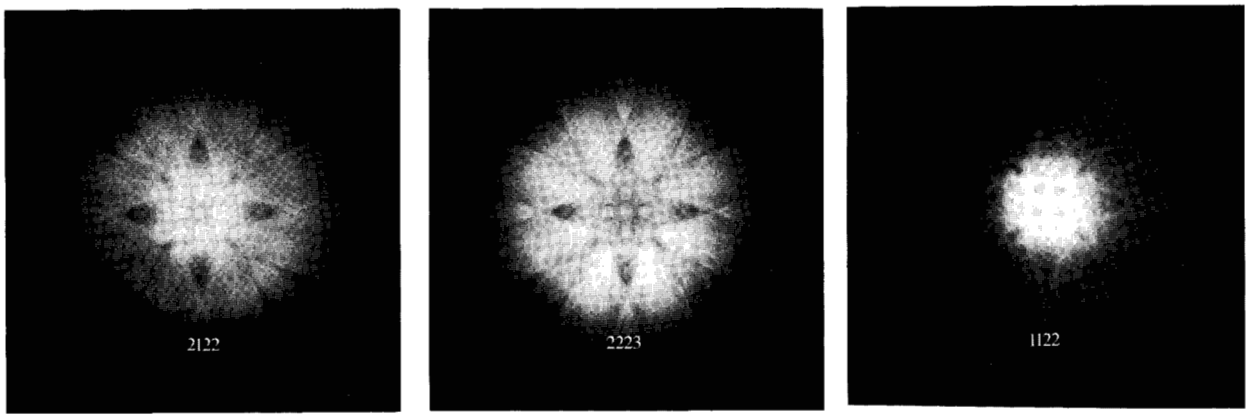

(a) (b) (c)

Figure 2

[001] convergent-beam electron diffraction patterns from (a) 2122, (b) 2223, and (c) 1122 crystals showing the tetragonal symmetry of each structure. Possible lowering of the symmetry by the superlattice modulations is not evident in these patterns.

Superstructures

Superlattice modulations occur in most of the Tl–Ca–Ba–Cu–O structures [10–12, 21, 24, 32, 35–37, 39, 46]; 1021 and 1324 are the only structures in which no modulations have been observed. For the other oxides, it is convenient to describe the modulations for pairs of structures because each pair has the same superlattice wave vector.

Figures 3(a)–3(c) show the [100], [110], and [001] selected area diffraction patterns of the 2122 structure. Weak superlattice reflections are evident around each of the fundamental reflections in the [100] and [001] patterns, but not in the [110] pattern. The [100] and [110] patterns indicate that the superlattice reflections seen in the [001] pattern are caused by a relrod effect. **Figure 3(d)** shows the distribution of satellite reflections in reciprocal space deduced from our electron diffraction studies of the 2122 structure [11, 12]. The intensity and sharpness of the satellite reflections varies from grain to grain. An identical distribution is found in the 2223 structure. The superlattice wave vectors for both of these structures are of the $\mathbf{k} = \langle 0.17, 0, 1 \rangle$ type. The possibility that each $\mathbf{k}$ corresponds to a different crystal variant with lowered symmetry remains unresolved.

Similar diffraction experiments (**Figure 4**) on the 1122 and 1223 structures yield the distribution of satellite reflections shown in Figure 4(c). The superlattice wave vectors for these two structures are of the $\mathbf{k} = \langle 0.29, 0, 0.5 \rangle$ type.

The most intense superlattice reflections occur in the 2021 polymorphs (**Figure 5**). The wave vector is the same in both polymorphs, but the notation used to describe it depends on the unit cell setting. The approximate wave vector is $\mathbf{k} = \langle \overline{0.16}, 0.08, 1 \rangle$ in the tetragonal $a_p \times a_p$ setting, whereas it is $\mathbf{k} = \langle \overline{0.08}, 0.24, 1 \rangle$ in the orthorhombic $2a_p \times 2a_p$ setting [Figure 5(d)]. The polymorphs were described above as *nominally* orthorhombic and tetragonal because taking the superlattice into account lowers the symmetry of both structures to monoclinic, with the c axis being the unique axis.

The superlattices in the thallium superconductors are distinct from those found in the related Bi–Ca–Sr–Cu–O superconductors and are much weaker in intensity. As for the bismuth superconductors, the source of these modulations is still being investigated. Local distortions in the Tl–O layers are believed to be the most probable cause.

Defect structures

The major defects in crystals with more than one Cu perovskite-like unit are intergrowths of related structures, each corresponding to the addition or deletion of a perovskite-like unit or a Tl–O layer from the predominant structure. The intergrowths can occur over a wide range of length scales. In some samples, intergrowths occur on a 5–10-μm scale and are easily detected in scanning electron microscope, electron microprobe, and Raman microprobe studies [11, 12, 29]. Numerous transmission electron microscope (TEM) studies revealed that intergrowths also occur on much finer scales [9–12, 21–23, 35, 43, 48, 49, 51, 53]. For example, **Figure 6(a)** shows a single grain containing both the 1223 and 1122 structures (upper and lower portions, respectively). The corresponding diffraction pattern consists of a superposition of the [010] patterns from the two structures **[Figure 6(b)]**.

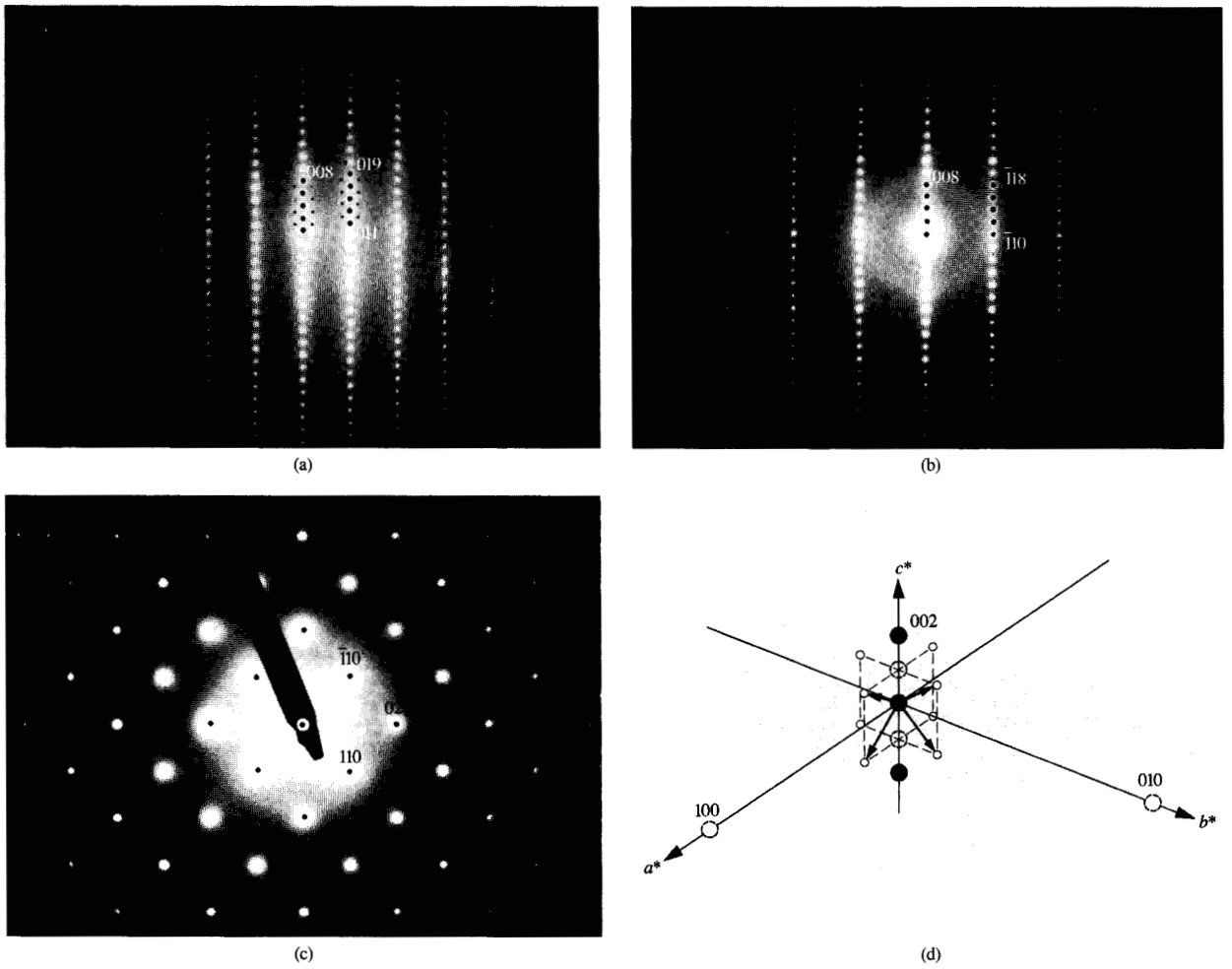

Figure 3

(a) [100], (b) [110], and (c) [001] selected area diffraction patterns from the body-centered tetragonal 2122 phase. (d) Schematic of the distribution of superlattice reflections about the fundamental reflections in 2122. The fundamental reflections are the large solid circles, while those that are systematically absent are the large dashed circles. The small open circles denote the superlattice reflections, and the bold arrows show the corresponding wave vectors. The same distribution is observed in 2223 [12].

In addition, intergrowths occur on a unit cell scale within the 1223 crystal [between the white arrows in Figure 6(a)]. The high-resolution TEM image in **Figure 6(c)** directly reveals a monolayer 1122 intergrowth in the 1223 structure.

The superconducting transition temperatures (T_c) in these crystals vary with the density of stacking defects. Resistivity and Meissner data established that T_c can take a range of values for all of the double and triple CuO_2 layer structures [12, 55]. For a given compound, X-ray diffraction and microprobe studies did not detect any obvious difference between the samples with different transition temperatures. TEM studies, however, showed a clear correlation between the density of intergrowths and T_c. For example, we found that defect-free 2223 crystals have a T_c of 125 K, whereas 2223 crystals containing a high density of randomly distributed 2122 intergrowths have a T_c of only 118 K [9]. Similarly, randomly distributed 1122 intergrowths reduce the T_c of 1223 crystals from 110 K to 100 K and the T_c of 2122 crystals from 108 K to 95 K [11]. It is difficult to determine whether it is the local change in structure or composition produced by the intergrowths that affects the superconducting transition temperature, because these are concurrent changes.

The superconducting transition temperatures reported in the single CuO_2 layer compounds (2021 and 1021) vary over a much wider range than those found in the other structures (**Figure 7**), but intergrowth defects do not explain these variations. Hazen et al. [8] identified 2021 as the 80 K

superconductor in the Tl–Ba–Cu–O samples of Sheng and Hermann [6]. Torardi et al. [15] verified this result and found 2021 to be tetragonal with no superlattice modulations. On the other hand, the first 2021 samples we prepared were orthorhombic with superlattice modulations, but not superconducting [11]. Because of our previous experience with intergrowths in the other phases, we doped our 2021 samples with calcium with the expectation that 2122 intergrowths would form and the material would become superconducting above liquid nitrogen temperature. These samples did indeed reach zero resistance at ~100 K, but our microstructural studies revealed that this was due to the calcium segregating into 2122 as a minor second phase. Structural studies found that the 2021 crystals in these samples were tetragonal, not orthorhombic, and Meissner data indicated a T_c of <20 K, rather than the previously reported 80 K value. Using a copper-rich starting composition, 2 Tl: 2Ba: 2Cu, we subsequently made tetragonal 2021 samples without calcium, but we were not able to increase T_c substantially above 20 K [12]. Although it is now known that an orthorhombic-to-tetragonal transition (and not intergrowths) plays a key role in determining the superconducting properties of 2021, the precise structural differences between the 0, 20, and 80 K 2021 superconductors remain unknown.

Wide variations in the transition temperatures in materials with the 1021 structure may also occur: We determined that 1021 is not superconducting down to 4 K [11], but Haldar et al. [33] reported a superconducting onset temperature of 50 K in $(Tl,Bi)_1(Sr,Ca)_2Cu_1O_{4.5+x}$, which has the 1021 structure. Thus, from a scientific viewpoint, the most interesting thallium superconductors may turn out to be those with the lowest transition temperatures.

Site occupancy

It is clearly an idealization to treat these oxides as line compounds (see Table 1). The stacking defects are one way to accommodate off-stoichiometry in the metal cations. Microprobe analysis consistently finds excess thallium in the Tl–O monolayer phases, indicative of Tl–O bilayer intergrowths [11, 12]. Indeed, high-resolution TEM studies often report finding extra Tl–O layers in the Tl–O monolayer materials [10, 11, 48]. Conversely, microprobe analysis consistently finds thallium deficiency in the Tl–O bilayer phases, indicative of Tl–O monolayer intergrowths, yet few TEM studies have reported finding such defects in these materials [49]. The TEM results could be rationalized based on the fact that high-resolution studies examine an exceedingly small fraction of a given sample, which may not be representative of the sample, or they could point to deficiency on the thallium sites as an alternative explanation.

X-ray diffraction studies of small single crystals and neutron diffraction studies of powders have indeed found evidence for vacancies or calcium substitution on the

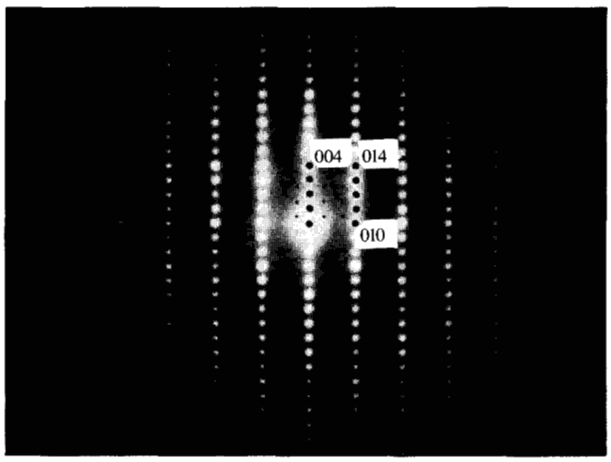

(a)

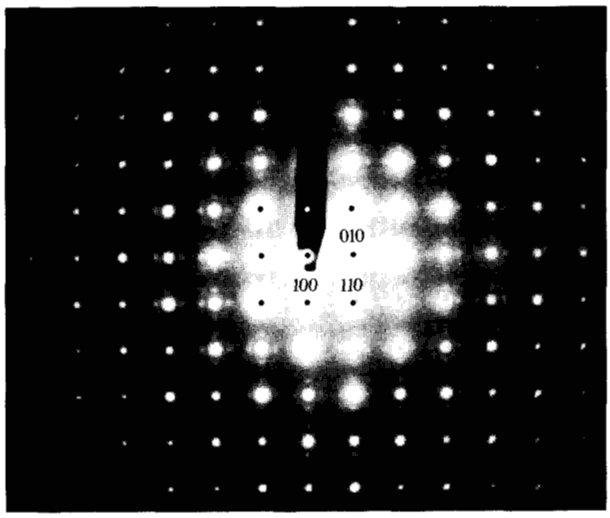

(b)

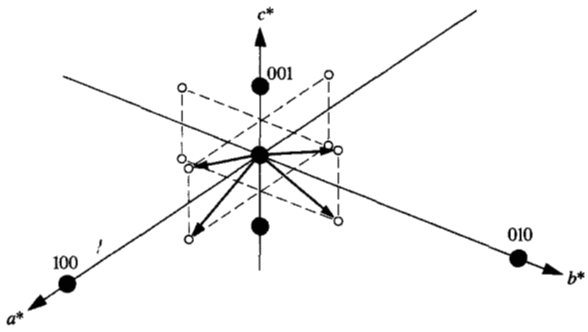

(c)

Figure 4

(a) [100] and (b) [001] selected area diffraction patterns from the primitive tetragonal 1122 phase. (c) Schematic of the distribution of superlattice reflections about the fundamental reflections in 1122. The same distribution is observed in 1223 [12].

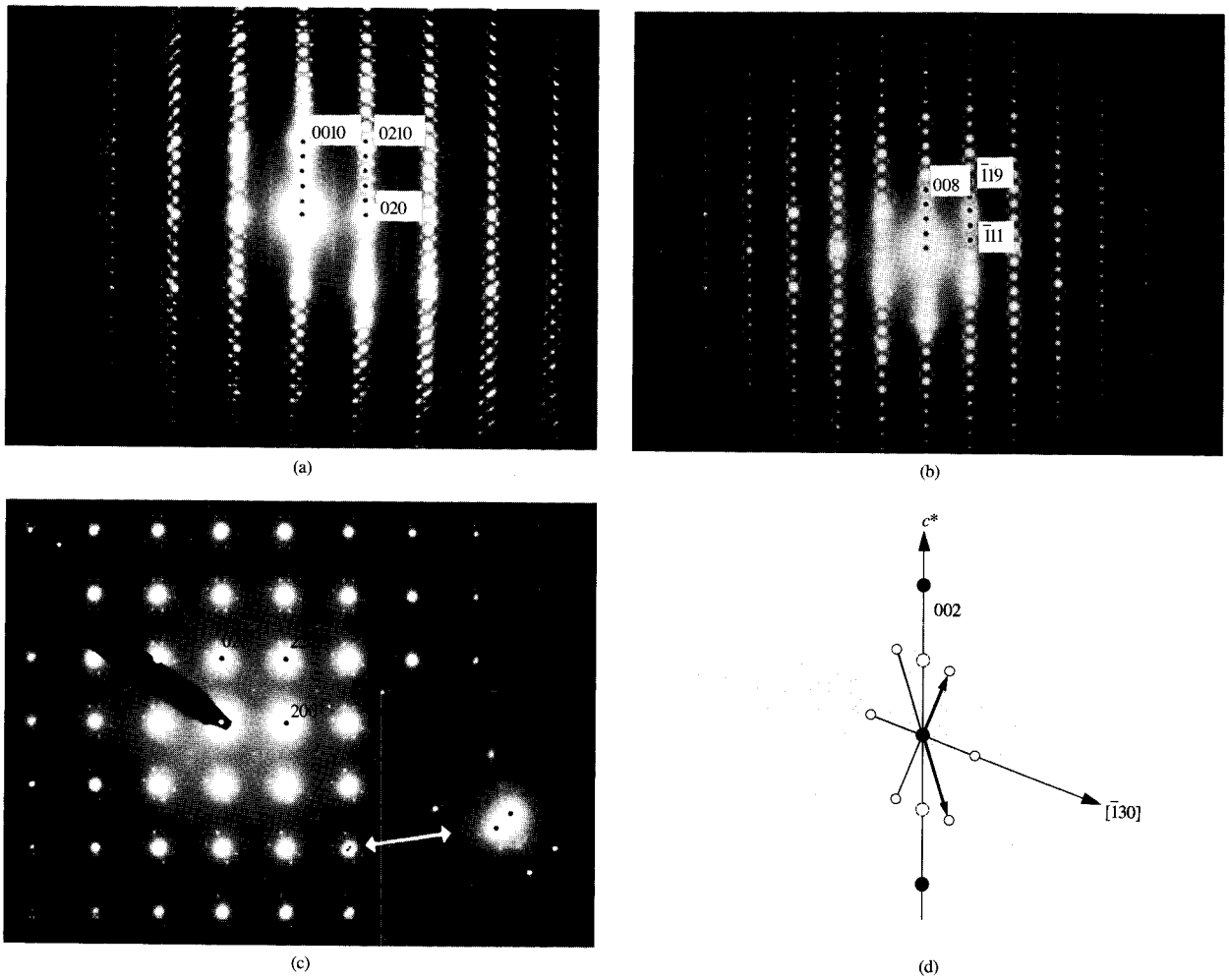

Figure 5

(a) [100], (b) [110], and (c) [001] selected area diffraction patterns from the face-centered orthorhombic 2021 polymorph. In (c) the distribution of superlattice and twin spots is enhanced for clarity in the inset. (d) Schematic of the distribution of superlattice reflections about the fundamental reflections in orthorhombic 2021. The same distribution is observed in the tetragonal polymorph, but it is more diffuse and the crystallographic notation used to describe it is different (see Table 1) [12].

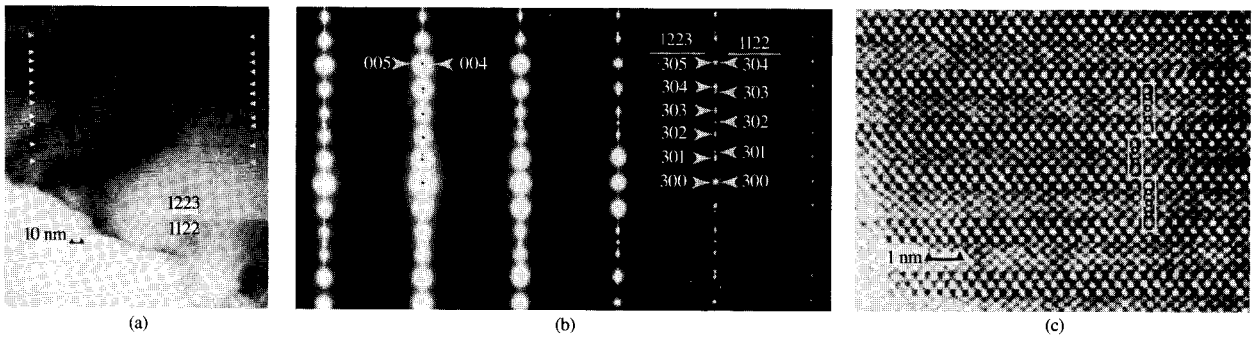

Figure 6

(a) Bright-field image of a grain containing both 1223 (upper) and 1122 (lower) intergrowths. The white arrows denote unit-cell thick 1122 intergrowths in the 1223 crystal. (b) The corresponding diffraction pattern is a superposition of [010] patterns from 1223 and 1122. (c) High-resolution image of a unit-cell thick 1122 intergrowth in 1223. The unit cells are outlined and the copper columns are marked within each cell [12].

thallium site, as well as thallium substitution on the calcium site, in the 2122 and 2223 structures [14, 16, 17, 37]. Similarly, powder neutron diffraction and TEM studies of the 2021 polymorphs by Hewat et al. [38, 39] concluded that there are ordered vacancies on one eighth of the thallium and oxygen sites, which give rise to the $\mathbf{k} = \langle \overline{0.08}, 0.24, 1 \rangle$ superlattice modulation and account for the thallium deficiency. However, a subsequent neutron diffraction study by Parise et al. [18] did not report any evidence for thallium deficiency in 2021. Thus, there is no consensus yet on the detailed features of the 2021 structure.

The absolute oxygen content and its variation with processing have not been determined precisely in any of these oxides. At present, the oxygen occupancy determined from diffraction studies appears to be close to its idealized value, and its variation is much less than that in $Y_1Ba_2Cu_3O_{7-x}$.

It is important to determine accurately the site occupancies in these materials in order to know what gives rise to the free carriers (holes). In $La_{2-x}Sr_xCuO_4$ and $Y_1Ba_2Cu_3O_{7-x}$, alkaline earth doping and oxygen doping, respectively, are used to create holes. A strong correlation is found between hole concentration and T_c in these materials: T_c increases with hole concentration up to an effective copper valence of ~2.25 and then declines thereafter [55–57]. It would be useful to determine whether the same trends occur in the thallium superconductors. The average Cu oxidation state in the *ideal* Tl–O monolayer structures varies from +2.25 in 1324 (T_c = 122 K) to +3 in 1021 (not superconducting). The average Cu oxidation state is +2 for all of the *ideal* Tl–O bilayer structures. The characterization work done thus far points toward thallium and/or calcium deficiency as the primary source of holes in the 2021, 2122, and 2223 phases. Note that only a few percent thallium deficiency can create a large number of holes in these materials.

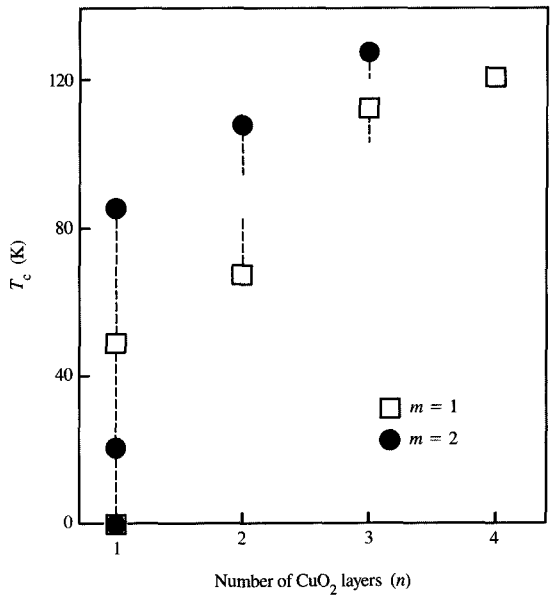

Figure 7

Superconducting transition temperature, T_c, versus the number of CuO_2 layers in the perovskite-like unit in $Tl_mCa_{n-1}Ba_2Cu_nO_{2(n+1)+m}$ (open squares for Tl–O monolayer structures, closed circles for Tl–O bilayer structures). The dashed vertical lines correspond to the variations in T_c reported for each phase [8, 12, 33, 40].

Concluding remarks

Initially there was very rapid progress in understanding Tl–Ca–Ba–Cu–O oxides. Researchers discovered seven different oxides and determined their basic crystallography, microstructure, and properties in a few short months. The structures of the thallium (and bismuth) superconductors show that the linear CuO_3 chains, twins, and orthorhombicity in the $Y_1Ba_2Cu_3O_{7-x}$ structure are not essential for superconductivity, leaving the CuO_2 planes as the key structural feature. The 1122 structure and the 2021 polymorphs are particularly compelling examples in this regard. The 1122 structure is essentially just the $Y_1Ba_2Cu_3O_{7-x}$ structure with the linear CuO_3 chains replaced by a Tl–O monolayer. For the 2021 polymorphs, the untwinned tetragonal form is superconducting, but the twinned orthorhombic form is not. The thallium superconductors also show that T_c increases with the number of CuO_2 layers in the perovskite-like unit. Earlier comparisons of the $Y_1Ba_2Cu_3O_{7-x}$ and $La_{2-x}M_xCuO_{4-y}$ structures led to speculation that this might be the case. Theorists are currently trying to explain this trend [58, 59], while experimentalists are trying to increase the number of CuO_2 layers. Preliminary studies indicate that additional CuO_2 layers may *decrease* T_c in both the Tl–O monolayer and bilayer series [60]. It is not clear, however, whether the conditions used to prepare these materials have optimized their superconducting properties.

We expect that continued progress in understanding and using thallium superconductors will be slowed by problems in preparing high-quality materials. Without a better understanding of the high-temperature chemistry, it will be difficult to prepare large crystals with few intergrowth defects. Such samples are needed to unambiguously determine the source of the superlattice modulations and the variations in metal cation and oxygen site occupancies, as well as the superconducting and normal state properties of each oxide. Without single phase samples prepared in controlled environments, it will be difficult to determine the effects of cation substitutions on structure and properties, as

has been done for $Y_1Ba_2Cu_3O_{7-x}$ [61]. Thus, significant advances in understanding structure-property relationships in the thallium superconductors will depend on advances in understanding processing-structure relationships.

Acknowledgments

We thank E. M. Engler, P. M. Grant, F. Herman, T. M. Shaw, R. Sinclair, and J. B. Torrance for useful discussions. We thank R. Karimi, M. L. Ramirez, K. P. Roche, and J. Vazquez for their technical support. We are grateful to Prof. R. Sinclair at Stanford University for the use of his electron microscope.

References

1. J. G. Bednorz and K. A. Müller, *Z. Phys. B* **64**, 189 (1986).
2. J. G. Bednorz, M. Takashige, and K. A. Müller, *Europhys. Lett.* **3**, 379 (1987).
3. M. K. Wu, J. R. Ashburn, C. J. Torng, P. H. Hor, R. L. Meng, L. Gao, Z. J. Huang, Y. Q. Wang, and C. W. Chu, *Phys. Rev. Lett.* **58**, 908 (1987).
4. H. Maeda, Y. Tanaka, M. Fukutomi, and T. Asano, *Jpn. J. Appl. Phys.* **27**, L209 (1988).
5. Z. Z. Sheng and A. M. Hermann, *Nature* **332**, 55 (1988).
6. Z. Z. Sheng and A. M. Hermann, *Nature* **332**, 138 (1988).
7. R. J. Cava, B. Batlogg, J. J. Krajewski, L. W. Rupp, L. F. Schneemeyer, T. Siegrist, R. B. van Dover, P. Marsh, W. F. Peck, Jr., P. K. Gallagher, S. H. Glarum, J. H. Marshall, R. C. Farrow, J. V. Waszczak, R. Hull, and P. Trevor, *Nature* **336**, 211 (1988).
8. R. M. Hazen, L. W. Finger, R. J. Angel, C. T. Prewitt, N. L. Ross, C. G. Hadidiacos, P. J. Heaney, D. R. Veblen, Z. Z. Sheng, A. El Ali, and A. M. Hermann, *Phys. Rev. Lett* **60**, 1657 (1988).
9. S. S. P. Parkin, V. Y. Lee, E. M. Engler, A. I. Nazzal, T. C. Huang, G. Gorman, R. Savoy, and R. Beyers, *Phys. Rev. Lett.* **60**, 2539 (1988).
10. S. S. P. Parkin, V. Y. Lee, A. I. Nazzal, R. Savoy, R. Beyers, and S. J. La Placa, *Phys. Rev. Lett.* **61**, 750 (1988).
11. R. Beyers, S. S. P. Parkin, V. Y. Lee, A. I. Nazzal, R. Savoy, G. Gorman, T. C. Huang, and S. La Placa, *Appl. Phys. Lett.* **53**, 432 (1988).
12. S. S. P. Parkin, V. Y. Lee, A. I. Nazzal, R. Savoy, T. C. Huang, G. Gorman, and R. Beyers, *Phys. Rev. B* **38**, 6531 (1988).
13. W. Y. Lee, V. Y. Lee, J. Salem, T. C. Huang, R. Savoy, D. C. Bullock, and S. S. P. Parkin, *Appl. Phys. Lett.* **53**, 329 (1988).
14. M. A. Subramanian, J. C. Calabrese, C. C. Torardi, J. Gopalakrishnan, T. R. Askew, R. B. Flippen, K. J. Morrissey, U. Chowdhry, and A. W. Sleight, *Nature* **332**, 420 (1988).
15. C. C. Torardi, M. A. Subramanian, J. C. Calabrese, J. Gopalakrishnan, E. M. McCarron, K. J. Morrissey, T. R. Askew, R. B. Flippen, U. Chowdhry, and A. W. Sleight, *Phys. Rev. B.* **38**, 225 (1988).
16. C. C. Torardi, M. A. Subramanian, J. C. Calabrese, J. Gopalakrishnan, K. J. Morrissey, T. R. Askew, R. B. Flippen, U. Chowdhry, and A. W. Sleight, *Science* **240**, 631 (1988).
17. D. E. Cox, C. C. Torardi, M. A. Subramanian, J. Gopalakrishnan, and A. W. Sleight, *Phys. Rev. B* **38**, 6624 (1988).
18. J. B. Parise, J. Gopalakrishnan, M. A. Subramanian, and A. W. Sleight, *J. Solid State Chem.* **76**, 432 (1988).
19. M. A. Subramanian, J. B. Parise, J. C. Calabrese, C. C. Torardi, J. Gopalakrishnan, and A. W. Sleight, *J. Solid State Chem.* **77**, 192 (1988).
20. W. Dmowski, B. H. Toby, T. Egami, M. A. Subramanian, J. Gopalakrishnan, and A. W. Sleight, *Phys. Rev. Lett.* **61**, 2608 (1988).
21. S. Iijima, T. Ichihashi, and Y. Kubo, *Jpn. J. Appl. Phys.* **27**, L817 (1988).
22. S. Iijima, T. Ichihashi, Y. Shimakawa, T. Manako, and Y. Kubo, *Jpn. J. Appl. Phys.* **27**, L837 (1988).
23. S. Iijima, T. Ichihashi, Y. Shimakawa, T. Manako, and Y. Kubo, *Jpn. J. Appl. Phys.* **27**, L1054 (1988).
24. S. Iijima, T. Ichihashi, Y. Shimakawa, T. Manako, and Y. Kubo, *Jpn. J. Appl. Phys.* **27**, L1061 (1988).
25. Y. Shimakawa, Y. Kubo, T. Manako, Y. Nakabayashi, and H. Igarashi, *Physica C* **156**, 97 (1988).
26. D. S. Ginley, E. L. Venturini, J. F. Kwak, R. J. Baughman, M. J. Carr, P. F. Hlava, J. E. Schirber, and B. Morosin, *Physica C* **152**, 217 (1988).
27. B. Morosin, D. S. Ginley, E. L. Venturini, P. F. Hlava, R. J. Baughman, J. F. Kwak, and J. E. Schirber, *Physica C* **152**, 223 (1988).
28. B. Morosin, D. S. Ginley, P. F. Hlava, M. J. Carr, R. J. Baughman, J. E. Schirber, E. L. Venturini, and J. F. Kwak, *Physica C* **152**, 413 (1988).
29. K. F. McCarty, D. S. Ginley, D. R. Boehme, R. J. Baughman, and B. Morosin, *Solid State Commun.* **68**, 77 (1988).
30. D. S. Ginley, J. F. Kwak, R. P. Hellmer, R. J. Baughman, E. L. Venturini, M. A. Mitchell, and B. Morosin, *Physica C* **156**, 592 (1988).
31. B. Morosin, D. S. Ginley, J. E. Schirber, and E. L. Venturini, *Physica C* **156**, 587 (1988).
32. J. D. Fitz Gerald, R. L. Whithers, J. G. Thompson, L. R. Wallenberg, J. S. Anderson, and B. G. Hyde, *Phys. Rev. Lett.* **60**, 2797 (1988).
33. P. Haldar, A. Roig-Janicki, S. Sridhar, and B. C. Giessen, *Mater. Lett.* **7**, 1 (1988).
34. P. Haldar, K. Chen, B. Maheswaran, A. Roig-Janicki, N. K. Jaggi, R. S. Markiewicz, and B. C. Giessen, *Science* **241**, 1198 (1988).
35. H. W. Zandbergen, G. Van Tendeloo, J. Van Landuyt, and S. Amelinckx, *Appl. Phys. A* **46**, 233 (1988).
36. H. W. Zandbergen, W. A. Groen, F. C. Mijlhoff, G. Van Tendeloo, and S. Amelinckx, *Physica C* **156**, 325 (1988).
37. A. W. Hewat, E. A. Hewat, J. Brynestad, H. A. Mook, and E. D. Specht, *Physica C* **152**, 438 (1988).
38. A. W. Hewat, P. Bordet, J. J. Capponi, C. Chaillout, J. Chenavas, M. Godinho, E. A. Hewat, J. L. Hodeau, and M. Marezio, *Physica C* **156**, 369 (1988).
39. E. A. Hewat, P. Bordet, J. J. Capponi, C. Chaillout, J. Chenavas, M. Godinho, A. W. Hewat, J. L. Hodeau, and M. Marezio, *Physica C* **156**, 375 (1988).
40. H. Ihara, R. Sugise, M. Hirabayashi, N. Terada, M. Jo, K. Hayashi, A. Negishi, M. Tokumoto, Y. Kimura, and T. Shimomura, *Nature* **334**, 510 (1988).
41. H. Ihara, R. Sugise, K. Hayashi, N. Terada, M. Jo, M. Hirabayashi, A. Negishi, N. Atoda, H. Oyanagi, T. Shimomura, and S. Ohashi, *Phys. Rev. B* **38**, 11952 (1988).
42. R. Sugise, M. Hirabayashi, N. Terada, M. Jo, T. Shimomura, and H. Ihara. *Jpn. J. Appl. Phys.* **27**, L1709 (1988).
43. K. K. Fung, Y. L. Zhang, S. S. Xie, and Y. Q. Zhou, *Phys. Rev. B* **38**, 5028 (1988).
44. J. K. Liang, Y. L. Zhang, J. Q. Huang, S. S. Xie, G. C. Che, X. R. Chen, Y. M. Ni, D. N. Zhen, and S. L. Jia, *Physica C* **156**, 616 (1988).
45. J. K. Liang, Y. L. Zhang, J. Q. Huang, S. S. Xie, C. C. Che, X. R. Chen, Y. M. Ni, and D. N. Zhen, *Z. Phys. B* **73**, 9 (1988).
46. Y. Liu, Y. L. Zhang, J. K. Liang, and K. K. Fung. *J. Phys. C: Solid State Phys.* **21**, L1039 (1988).
47. A. Sulpice, B. Giordanengo, R. Tournier, M. Hervieu, A. Maignan, C. Martin, C. Michel, and J. Provost, *Physica C* **156**, 243 (1988).
48. B. Domenges, M. Hervieu, and B. Raveau, *Solid State Commun.* **68**, 303 (1988).
49. M. Hervieu, C. Martin, J. Provost, and B. Raveau, *J. Solid State Chem.* **76**, 419 (1988).
50. S. J. Hibble, A. K. Cheetham, A. M. Chippindale, P. Day, and

J. A. Hriljac, *Physica C* **156**, 604 (1988).
51. J. P. Zhang, D. J. Li, H. Shibahara, and L. D. Marks, *Supercond. Sci. Technol.* **1**, 132 (1988).
52. K. Hiraga, D. Shindo, M. Hirabayashi, M. Kikuchi, N. Kobayashi, and Y. Syono, *Jpn. J. Appl. Phys.* **27**, L1848 (1988).
53. M. Verwerft, G. Van Tendeloo, and S. Amelinckx, *Physica C* **156**, 607 (1988).
54. M. Hong, S. H. Liou, D. D. Bacon, G. S. Grader, J. Kwo, A. R. Kortan, and B. A. Davidson, *Appl. Phys. Lett.* **53**, 2102 (1988).
55. M. W. Shafer, T. Penney, and B. L. Olson, *Phys. Rev. B* **36**, 4047 (1987).
56. J. B. Torrance, Y. Tokura, A. I. Nazzal, A. Bezinge, T. C. Huang, and S. S. P. Parkin, *Phys. Rev. Lett.* **61**, 1127 (1988).
57. Y. Tokura, J. B. Torrance, T. C. Huang, and A. I. Nazzal, *Phys. Rev. B* **38**, 7156 (1988).
58. R. V. Kasowski, W. Y. Hsu, and F. Herman, *Phys. Rev. B* **38**, 6470 (1988).
59. T. Schneider and D. Baeriswyl, *Z. Phys. B* **73**, 5 (1988).
60. H. Ihara, private communication.
61. See R. Beyers and T. M. Shaw, in *Solid State Physics, Advances in Research and Applications*, Vol. 42, H. Ehrenreich and D. Turnbull, Eds., Academic Press, Inc., New York, 1989, p. 135 and the references therein.

Received January 16, 1989; accepted for publication February 16, 1989

Robert B. Beyers *IBM Research Division, Almaden Research Center, 650 Harry Road, San Jose, California 95120.* Dr. Beyers received the B.S. degree in chemical engineering in 1980, the M.S. degree in materials science in 1982, and the Ph.D. degree in materials science in 1989, all from Stanford University. In his thesis research, he studied the formation and oxidation of metal silicide thin films in integrated circuits. He joined the Materials Science Department at the IBM Almaden Research Center in 1986. Dr. Beyers' research at IBM has focused on understanding processing-structure-property relationships in superconducting oxides.

Stuart S. P. Parkin *IBM Research Division, Almaden Research Center, 650 Harry Road, San Jose, California 95120.* Dr. Parkin is currently a Research Staff Member at the IBM Almaden Research Center. He was elected to a Research Fellowship at Trinity College, Cambridge, in 1979 and received his Ph.D. a year later. This work at the Cavendish Laboratory, Cambridge, involved studies of the structural and physical properties of a family of layered magnetic compounds. After a Royal Society European Exchange Fellowship at the Laboratoire de Physique des Solides, Orsay, France, Parkin joined the IBM Almaden Research Center in 1982. He was a member of the team that discovered a new class of organic superconductors (based on the BEDT-TTF molecule) in 1983. More recently, Dr. Parkin's interests have expanded to include research on the growth and properties of ultrathin magnetic films and superlattices. This work includes studies of the magnetization profiles of thin magnetic films using polarized neutron reflectometry and finite size effects on the magnetic properties of ultrathin antiferromagnetic films. After the discovery in 1986 of high-temperature superconductivity by Bednorz and Müller at the IBM Zurich Laboratory, Parkin joined the Almaden Research Center's effort, which has concentrated on studying the relationship of the materials' structures to their superconducting properties. One result of this effort has been the discovery of the compound with the highest known superconducting transition temperature and a new class of compounds in the Tl-Ca-Ba-Cu-O system.

Victor Y. Lee *IBM Research Division, Almaden Research Center, 650 Harry Road, San Jose, California 95120.* Mr. Lee received his B.S. in biochemistry from U.C. Berkeley in 1974 and his M.S. degree in chemistry in 1977 from San Jose State University. He has been involved in the synthesis of sulfur and selenium heterocyclic molecules showing conducting and superconducting properties. Mr. Lee's recent research interests include high-temperature superconductors in ceramic compounds and the crystal growth of organic compounds with nonlinear optical properties.

Adel I. Nazzal *IBM Research Division, Almaden Research Center, 650 Harry Road, San Jose, California 95120.* Mr. Nazzal received the B.S. degree in chemistry from San Jose State in 1971. He joined the IBM Research Center in San Jose in the Physical Science Department in 1974. At IBM, he has worked on a wide variety of synthetic chemical problems, including the syntheses of materials for charge-transfer reactions, liquid crystals, conducting polymers, materials for solar energy application, and organic ferromagnetic materials. Since 1987, Mr. Nazzal has been working on high-temperature superconductors.

Richard J. Savoy *IBM Research Division, Almaden Research Center, 650 Harry Road, San Jose, California 95120.* Mr. Savoy joined IBM Research in 1978. He is currently a Senior Associate Scientist in the Micro, Surface, and Analytical Science Department. His research interests at IBM have included magnetic recording materials, optical storage materials, and superconducting oxides.

Grace Lim Gorman *IBM Research Division, Almaden Research Center, 650 Harry Road, San Jose, California 95120.* Ms. Gorman is a Senior Associate Scientist/Engineer in the Micro, Surface, and Analytical Science Department. She received her B.S. in physics from the University of Hawaii in 1981 and her M.S. in physics from San Jose State University in 1985. Ms. Gorman joined IBM in 1981 and has since been working in the field of X-ray analysis. Her research interests include materials for optical and magnetic recording applications.

Ting C. Huang *IBM Research Division, Almaden Research Center, 650 Harry Road, San Jose, California 95120.* Dr. Huang is a Research Staff Member in the X-Ray Analysis Project of the Micro, Surface, and Analytical Science Department. He received his B.S. and M.S. degrees in electrical engineering from the Cheung-Kung University, Taiwan, in 1964 and 1966, respectively. Dr. Huang came to the United States in 1968 and obtained his Ph.D. degree in physics from the Polytechnic Institute of Brooklyn in 1972. Afterward, he spent one year as a Postdoctoral Fellow at IBM Burlington, Vermont, subsequently joining the IBM San Jose Research Laboratory in 1973. Dr. Huang was co-recipient of an IBM Outstanding Contribution Award for "Automated X-Ray Powder Diffraction Analysis" in 1974, and an IBM Research Division Outstanding Contribution Award for "Series/1 X-Ray Analysis Automation Products" in 1979. He also received a JCPDS Certificate Award in recognition of significant contribution to the Powder Diffraction File from the International Centre for Diffraction Data in 1988. Dr. Huang is a member of the American Crystallographic Association and the Joint Committee on Powder Diffraction Standards–International Centre for Diffraction Data; he is an editor of *Advances in X-Ray Analysis.*

Sam J. La Placa *IBM Research Division, T. J. Watson Research Center, P.O. Box 218, Yorktown Heights, New York 10598.* Mr. La Placa received a B.Sc. degree in chemistry from the Polytechnic Institute of New York, Brooklyn, in 1957. He was initially at the Brookhaven National Laboratory, and late in 1974 joined the IBM T. J. Watson Research Center as a Research Staff Member. His research on crystal structures of oxide superconductors uses both X-ray and neutron diffraction. Mr. La Placa's earlier work has included the study of low-dimensional electronic and ionic conductors, diffraction at high pressures, and quantum-mechanical modeling of X-ray diffraction measurements.